

Containment and penetration simulation in case of blade loss in a low pressure turbine

Astrid Kraus, Jörg Frischbier

MTU Aero Engines GmbH, Munich, Germany

Summary:

Blade failure in compressors and turbines at high rotational speeds is a critical event in aircraft engines. The aviation authority regulations require that containment of the blade loss is provided by the casing structure of the respective component, which has to be demonstrated by experiments or analysis. In the case of low pressure turbines, the containment capability can be verified analytically. The procedure established for containment design involves an energy balance method based on the comparison of the kinetic energy of the released blade and the strain energy of the containment zone. In addition, LS DYNA simulations are introduced for the analysis of the safety of blade containment in turbine casings. These allow for the consideration of several crucial effects that cannot be assessed with the conventional energy balance methods (structure of the released blade such as shroud and shank shape, influence of the adjacent blades, type of failure at impact, material behavior at high strain rates). Possible applications of LS DYNA containment simulations include optimization of an existing casing design such as minimizing the containment thickness to achieve weight reduction.

Keywords:

LS DYNA Simulation, containment, blade loss, low pressure turbine

1 Introduction

The failure of rotating parts such as blades or discs at high rotational speeds is a critical event in aircraft engines. In case of compressor or turbine blade failure, all fragments must be contained inside the casing structure. This requirement is described in detail in the specification, e.g. for blade loss in a low pressure turbine: “The LPT housing shall be designed to contain one (1) blade and that part of the blade fixing above the outermost fixing serration.” The engine containment capability must be demonstrated by test or analysis as prescribed by the aviation authorities. In case of low pressure turbines, it can be verified analytically. The established design procedure to determine the minimum casing wall thickness is an energy balance method based on the comparison of the kinetic energy of the released blade and the ultimate strain energy of the affected casing containment zone [Belohradsky, 1999]. The LS DYNA simulation are introduced as an additional tool to account for local special effects that cannot be assessed with the energy balance methods such as the influence of the remaining blading or strain rate dependent material properties. The application presented here is aiming at the optimization of a low pressure turbine demonstrator casing with respect to a possible engine application. The LS DYNA simulation of the blade loss event should yield a prediction of the containment capability and a recommendation of a minimum casing wall thickness (for weight reduction purposes) still satisfying the containment requirements. To identify the crucial effects in the simulation, sensitivity studies are carried out. The influence of the remaining blades on the momentum transfer is investigated in two steps. First a single blade failure is considered with no other blades contained in the model (“free blade loss”), secondly the adjacent blades are included. Three different containment thicknesses are evaluated in the containment zone. The material model is varied with respect to the failure criterion and strain rate effects. Turbine blade containment simulations using LS DYNA have already been carried out by [Atluri, 1996].

2 Description of the model

2.1 Geometry and boundary conditions

The LS DYNA model for the simulation of the blade loss event consists of the low pressure turbine casing and the respective blades as illustrated in Fig. 1. For the casing, three different containment thicknesses are investigated – the original thickness of 7mm and two configurations with reduced thicknesses of 5 mm and 3.6 mm in the containment zone.

For the first step of the single blade failure, the blade model includes the airfoil with outer shroud and shank and the fir tree attachment, the disc segment is left out. The specification requires containment of “one blade and that part of the blade fixing above the outermost fixing serration”, so the blade is released with outer shroud and inner diameter shank, but without the fir tree attachment. In the second step, the remaining blading of the stage is represented by the adjacent blades attached to disc segments (Fig. 2). These parts are modeled as rigid bodies in order to save computational costs.

The casing model and the blade to be released are meshed with eight-node solid hexahedron elements. The entire model with the axially symmetric casing and the blades contains up to 246000 nodes and 192000 solid elements (360 elements over the perimeter of the casing). There are six rows of elements through the casing thickness in the containment zone (Fig. 2). The elements in the blade and in the containment zone are assigned the fully integrated solid element formulation in order to avoid hourglassing. For the remaining elements in the casing model, a one-point integration constant stress element formulation is specified which reduces the computing time. The rigid bodies are modeled with one layer of shell elements representing the contact surface.

The interaction between the released blade and the casing and the adjacent blades is described with the “eroding_nodes_to_surface” contact option (type 16) with the blade nodes defined as slave. A contact surface is applied to each of the six layers through thickness in the containment zone in order to allow for material erosion. All contacts are assumed to be frictionless due to unknown coefficients of friction.

The casing is clamped at both flanges with all three translatory degrees of freedom set to zero representing the assembled condition. An initial velocity is assigned to the whole blade, it is forced on a circular path by applying the rotational speed to the fir tree attachment.

2.2 Material models

The low pressure turbine casing is to be made of a cast nickel based alloy. For both the blade and the casing, isotropic elastic-plastic material models with bilinear stress-strain curves are used. To study the influence of the material model, two different LS DYNA models are applied to the casing, in fact

the MAT3 (mat_plastic_kinematic) and the MAT17 (mat_oriented_crack) option. Strain rate effects are accounted for with the Cowper and Symonds model in case of the MAT3 option and by enhancing the yield stress in case of the MAT17 option. The true local failure strain and the ultimate stress are entered as limits for the failure criteria.

For the blade, attention has to be paid to the pace of element erosion resulting from the respective material model. If the blade mass is reduced too drastically due to element erosion, the transferred momentum might not be representative of the blade any more.

3 Results

Approximately one-quarter revolution is simulated after the blade release to cover the impact process. Therefore, effects such as secondary damage of the remaining blading or casing deformation due to an unbalanced rotor resulting from a blade loss cannot be assessed with the current simulations. The state of the released blade is shown without and with adjacent blades after $t = T/5$ in Fig. 3 and Fig. 4, respectively. The blade is rotating at maximum speed (redline speed) prior to the release. It is released by deleting the part representing the fir tree attachment. CPU time for the simulation of one-quarter revolution is approximately 200 hours in a single processor application on an SGI. The minimum time step size amounts to $1.0 \cdot 10^{-8}$ seconds.

In the following, the above mentioned case studies are discussed. For comparison of the different standards, the effective plastic strain is taken as a measure for the extent of the casing damage.

3.1 Blade loss simulated without and with adjacent blades

The single blade failure with no other blades included in the model and the one with adjacent blades are compared for the minimum casing thickness investigated (3.6 mm). In case of a free blade release, the failure strain is exceeded locally and the casing is penetrated. With the adjacent blades included, the blade loss is contained. In this case, the kinetic energy of the fragment increases considerably as it is impacted by the following blade (Fig. 5). However, the normal component of the momentum transferred to the casing decreases as a consequence of this impact. The maximum effective plastic strain in the containment zone reaches only about 15 percent of the failure strain (Fig. 6).

3.2 Comparison of different containment thickness

For comparison of different containment thicknesses, the more severe case of a single blade release is considered. In fact, the "free" blade loss is not contained for all three thicknesses evaluated. As expected, the maximum effective plastic strain is decreasing with increasing casing thickness. For the maximum investigated thickness (7 mm), penetration is predicted noticeably later (Fig. 7) and fewer elements are eroded (Fig. 8). With the maximum thickness, the casing can absorb much more energy. For the reduced thicknesses, penetration occurs at approximately the same time (Fig. 7). This indicates that raising the containment thickness and with it the overall casing stiffness might not boost the containment capability to the same extent. In case of excessive casing deformations the thinner casing offering higher flexibility might be more favorable.

3.3 Variation of the material characteristics

3.3.1 Influence of strain rate effects

The sensitivity of the simulation result towards a change in material behavior at high strain rates is investigated by including the rate effects in the MAT3 material model. For the casing with the minimum thickness, a material option with no strain rate dependency (curve 1) is compared to an option with a strong dependency (curve 2). For the second case, the Cowper and Symonds parameters are set such that the yield stress at $d\varepsilon/dt = 1000 \text{ s}^{-1}$ is increased by a factor of 1.7 compared to the static yield stress. Estimates show that the strain rate is of the order of magnitude of a 1000 s^{-1} at the impact examined here. The two curves are shown in Fig. 9, illustrating that the strain energy of the casing is much higher for the second option. While the casing is penetrated for the material option representing the "static" stress-strain curve (curve 1), the blade loss is contained in case of the enhanced yield stress (Fig. 10) with the maximum effective plastic strain reaching about 75 percent of the failure strain.

The consideration of strain rate effects in the simulation is a key factor as the applied casing material shows a strong general strain rate dependency in ballistic tests. Specific tests are planned to measure material properties such as the yield stress as a function of high strain rates.

1.1.2 Influence of different material models on the failure mode

In a typical blade loss accident, two principal failure modes can be observed [Dewhurst, 1991]:

- failure due to compression and shearing of the material over the impacted area
- failure due to the high local tensile strain exceeding the ultimate strain to failure of the material.

With the failure criterion integrated in the MAT3 material model (maximum effective plastic strain has to be specified), exceeding the ultimate strain in compression or tension leads to failure. In the second material model used for the casing (MAT17), element failure is only associated with tensile stresses and strains. For the situation investigated here (thin casings, distributed loads, moderate normal impact velocities), the second type of failure and hence the MAT17 material model seem to be more representative (only tensile failure with element erosion starting from the outside of the casing).

4 Summary

With the simulations carried out so far, the critical factors for the containment capability of the turbine casing can be determined. The fragmentation of the released blade is decisively different with and without the adjacent blades included in the analysis. To confirm their influence, the simulations have to be repeated with an elastic model of the adjacent blades. The use of an appropriate material model is crucial to the representation of the expected failure mode. Whether the material models considered in this simulations are suitable still needs to be validated with ballistic tests for the specific material. If strong strain rate dependence is observed for the material of interest, it should be considered in the simulation with a suitable material model.

In conclusion, the following benefits from the LS DYNA simulation in addition to the energy balance methods can be identified despite some uncertainties in the analyses:

- the interaction with the remaining blading can be investigated
- the simulation accounts for local effects (concentrated impact, local failure)
- the material behavior at high strain rates can be considered
- recommendations for the optimization of the casing design can be derived
- the simulation of multiple wall penetration events is possible.

5 Outlook

The LS DYNA simulations are to be verified with test results available from a blade-off spin rig test. Components considered in the test include the respective casing (turbine exhaust casing), the bladed disc, the up-stream vane and the liner, which is connected to the vane and contributes to the containment (Fig. 11 bottom). The test has demonstrated safe containment of the released blade at red line speed. The inner part of the casing (liner, not segmented) is penetrated, but all fragments are contained within the outer turbine casing (Fig. 11 top). The outer casing is only subjected to plastic deformation (visible bulge due to impact of the released blade, Fig. 12 right). No through cracks are detected in the post-test inspection.

With the LS DYNA analysis, the major test results should be reproduced. The effects of the multiple interactions between the liner, the outer casing and the released blade are represented in the model through appropriate contact definitions. The penetration of the liner (Fig. 11 bottom) as well as the plastic deformation of the outer casing resulting in a bulge (Fig. 12 left) should be predicted by the simulation. Moreover, the adjacent blades and the disc will be modeled as elastic parts.

6 References

Belohradsky H.-J.: "Blade-Containment: Berechnung der Durchschlagsicherheit von Flugtriebwerksgehäusen gegenüber Verdichter- und Turbinenleitschaufeln", MTU 1999.

Dewhurst T.B.: "The impact load on containment rings during a multiple blade shed in aircraft gas turbine engines", ASME 91-GT-163, 1991, 1-7.

Sarkar S., Atluri S.N.: "Effects of multiple blade interaction on the containment of blade fragments during a rotor failure", Finite Elements in Analysis and Design Vol.23, 1996, 211-223.

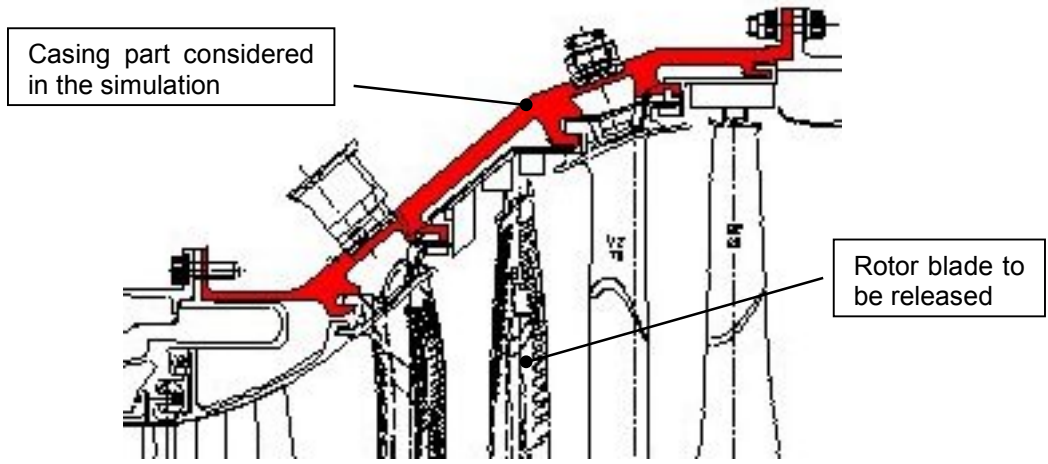


Fig. 1: Parts included in the containment simulation model

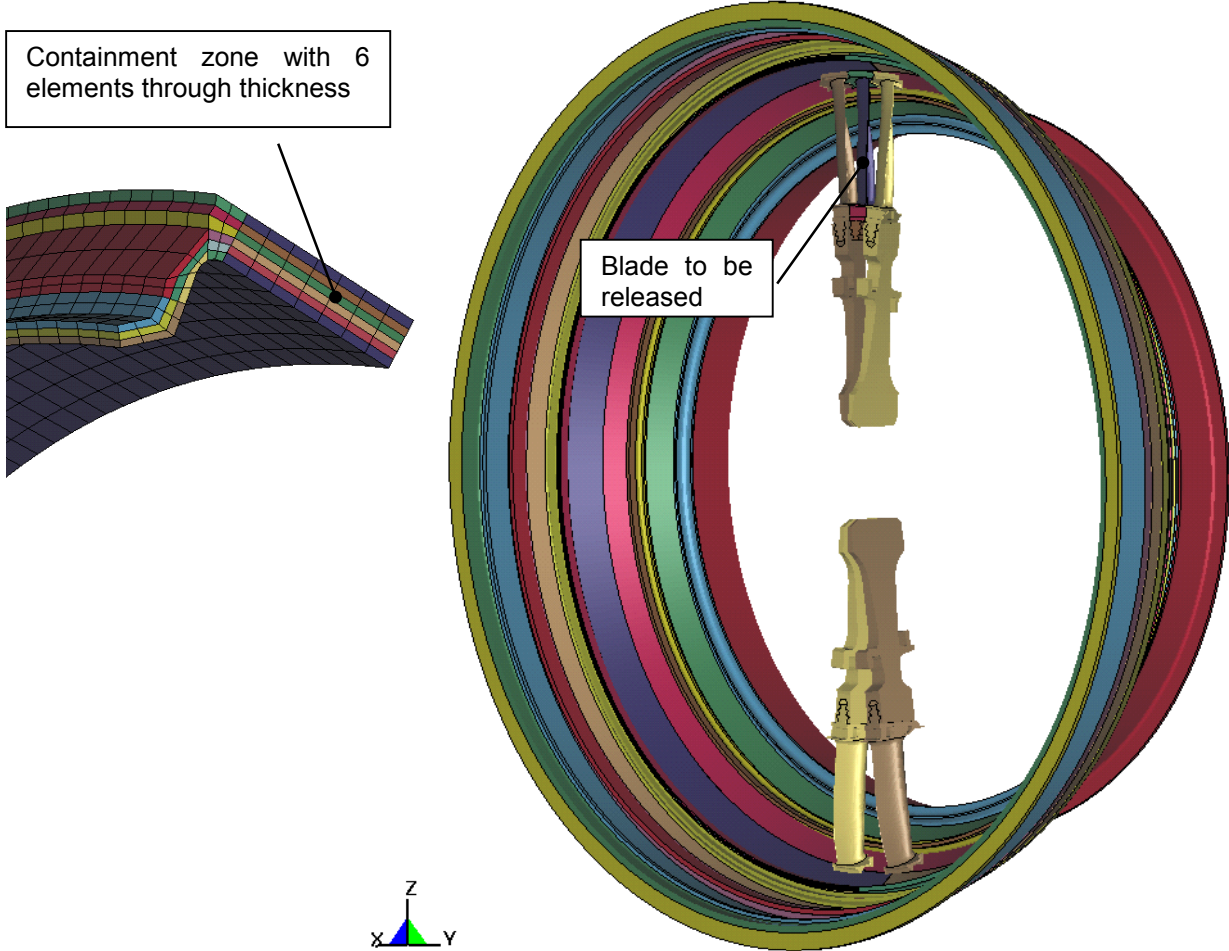


Fig. 2: Casing model with blade to be released and adjacent blades; detail of the containment zone

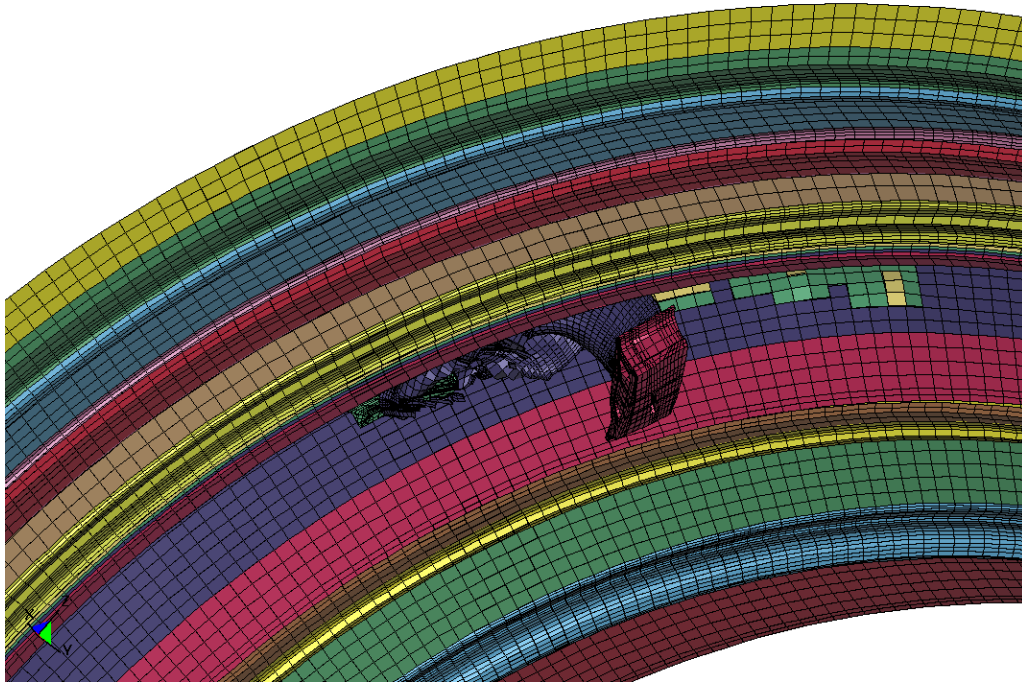


Fig. 3: Single blade release after $t = T/5$

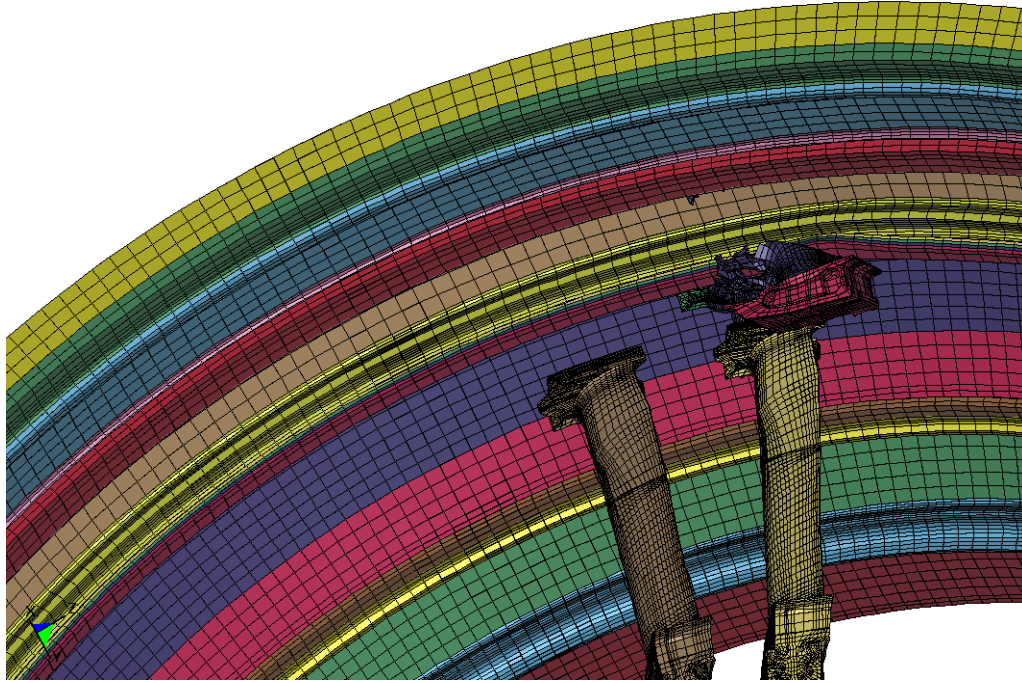


Fig. 4: Blades release with adjacent blades after $t = T/5$

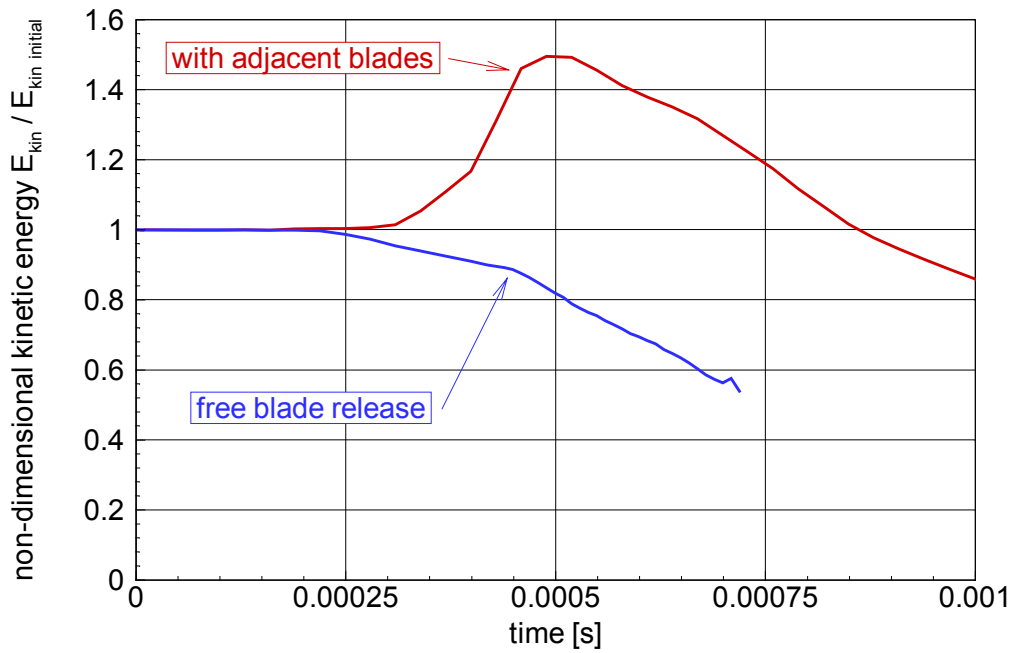


Fig. 5: Non-dimensional kinetic energy (over initial kinetic energy) for the blade released without and with adjacent blades (casing thickness 3.6 mm)

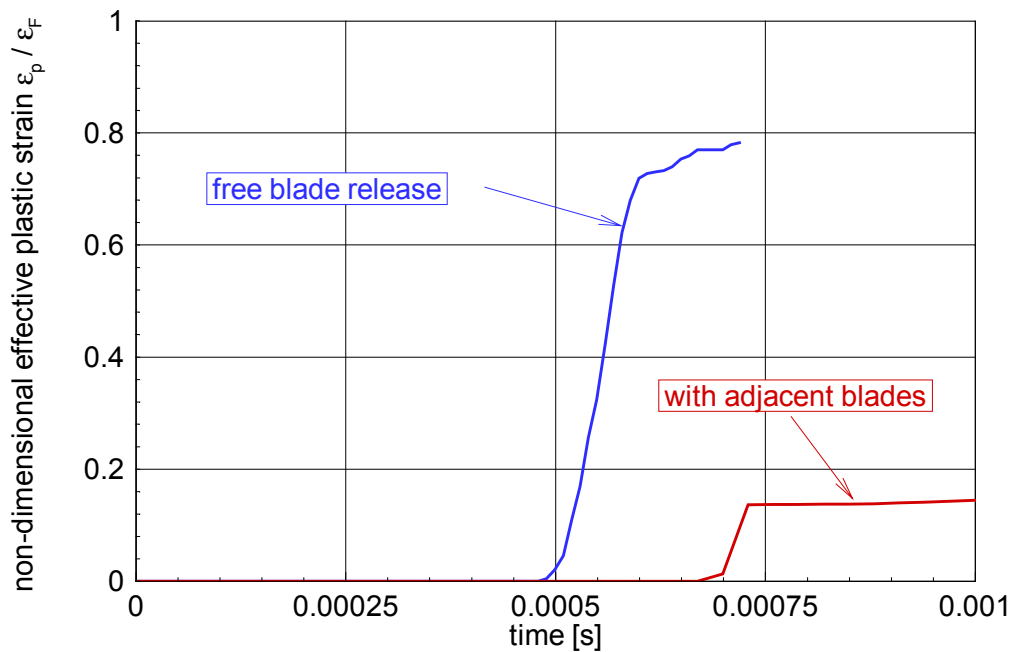


Fig. 6: Non-dimensional effective plastic strain (over failure strain) in the casing for a blade released without and with adjacent blades (casing thickness 3.6 mm)

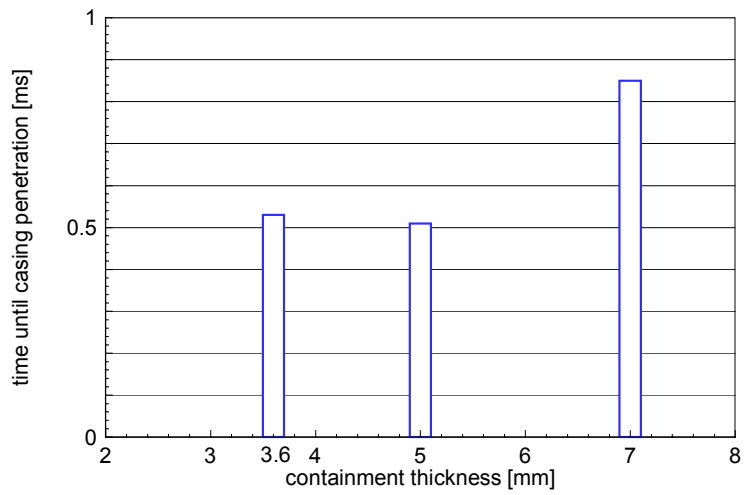


Fig. 7: Time until casing penetration in case of single blade release for different containment thickness

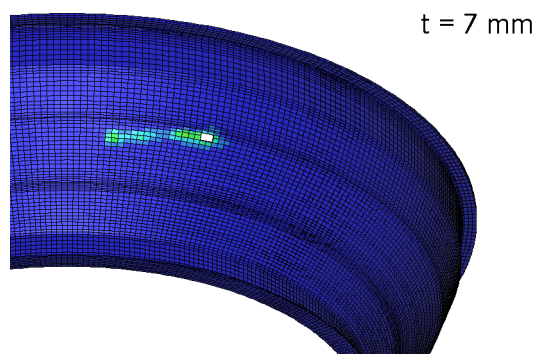
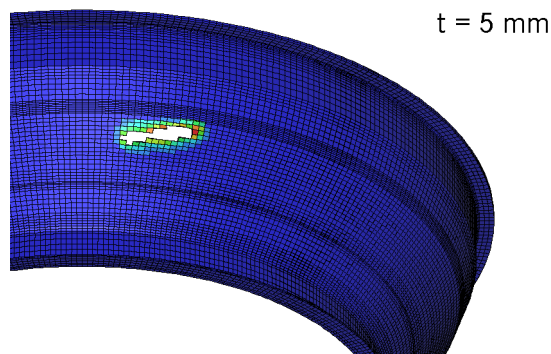
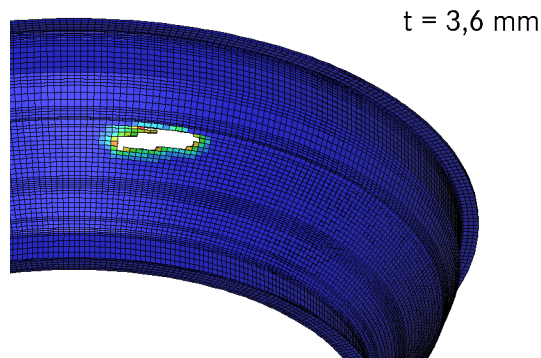


Fig. 8: Influence of casing thickness on effective plastic strain and number of failed elements

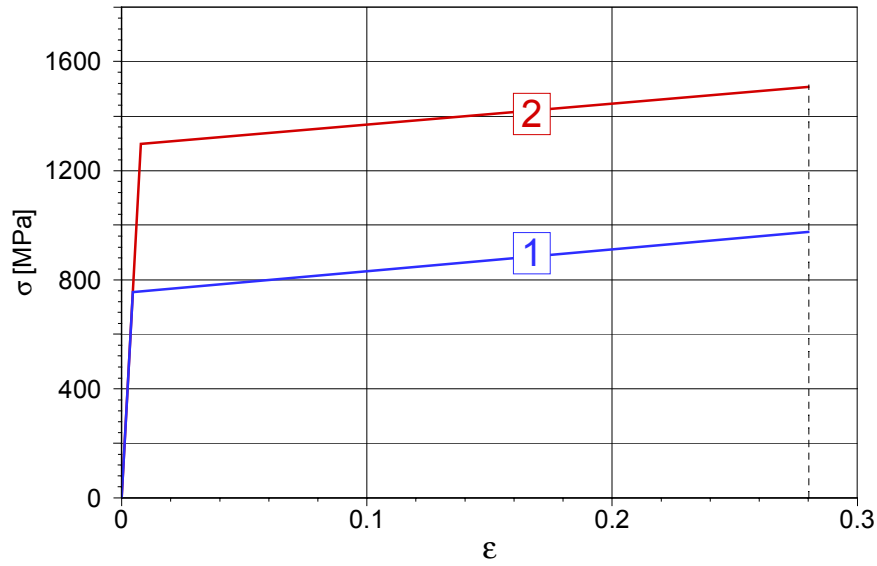


Fig. 9: Static stress-strain curve (1) and rate-dependent stress-strain curve (2) displayed for $d\varepsilon/dt = 1000 \text{ s}^{-1}$

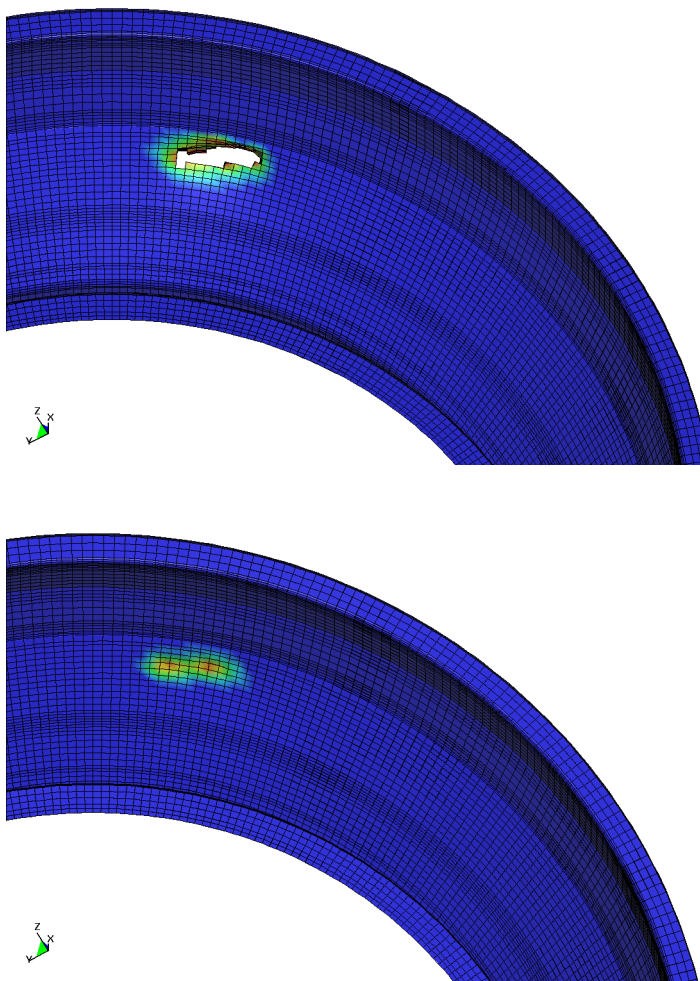


Fig. 10: Effective plastic strain and element erosion calculated without (top - curve 1 Fig. 9) and with (bottom - curve 2 Fig. 19) a strain rate dependency of the material

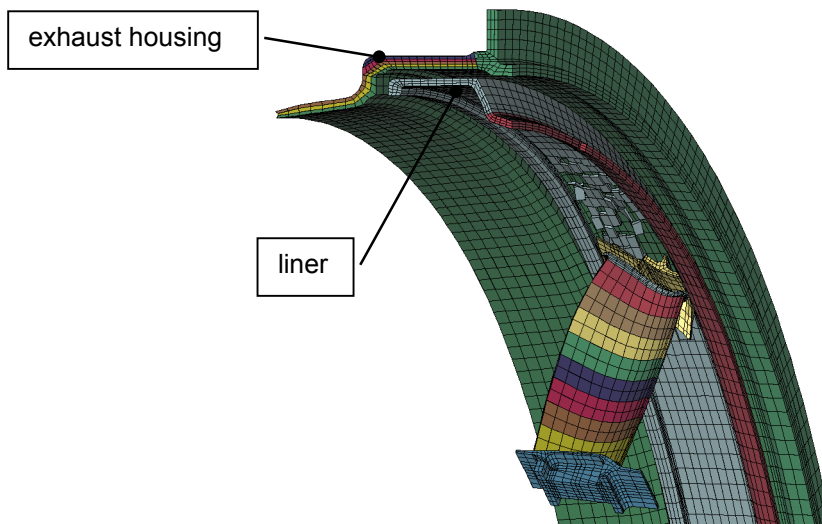
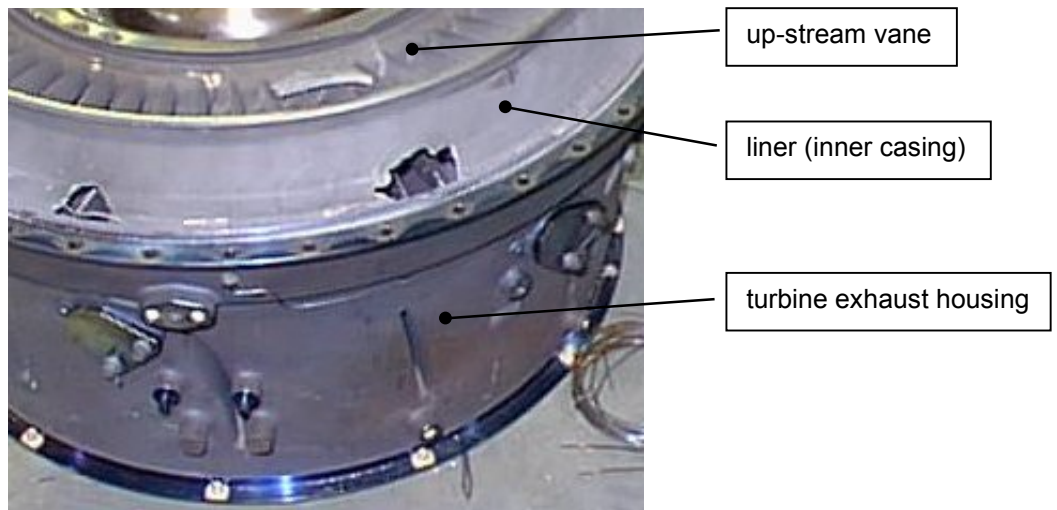


Fig. 11: Penetration of the liner in the blade-off rig test (top) and in the LS DYNA simulation (bottom)

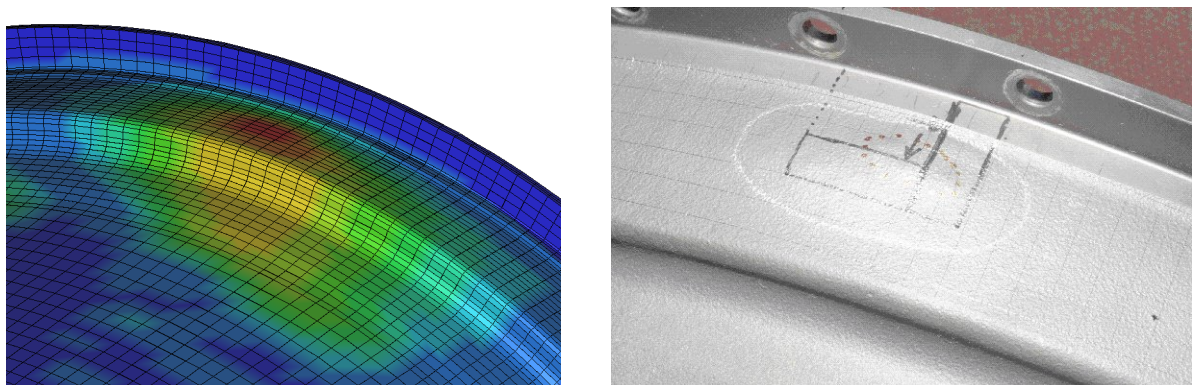


Fig. 12: Bulge in the exhaust housing due to impact of the released blade in the blade-off rig test (right) and in the LS DYNA simulation (left – resultant displacement)